Encapsulation of Size-Selected Ru_3 Clusters into RF-Deposited TiO_2

Liam Howard-Fabretto[1,2], Timothy J. Gorey[3], Guangjing Li[3], Siriluck Tesana[4], Gregory F. Metha[5], Scott L. Anderson[3], and Gunther G. Andersson[1,2]*

1 Flinders Institute for Nanoscale Science and Technology, Flinders University, Adelaide, South Australia 5042, Australia

2 Flinders Microscopy and Microanalysis, College of Science and Engineering, Flinders University, Adelaide, South Australia 5042, Australia

3 Chemistry Department, University of Utah, 315 S. 1400 E., Salt Lake City, UT 84112, United States

4 The MacDiarmid Institute for Advanced Materials and Nanotechnology, School of Physical and Chemical Sciences, University of Canterbury, Christchurch 8141, New Zealand

5 Department of Chemistry, University of Adelaide, Adelaide, South Australia 5005, Australia

*Corresponding author: Gunther G. Andersson

Email: gunther.andersson@flinders.edu.au.

Address: Physical Sciences Building (2111) GPO Box 2100, Adelaide 5001, South Australia

Abstract

In this study Ru_3 clusters are deposited onto radio frequency-sputter deposited TiO_2 (RF-TiO_2) substrates by both solution submersion and chemical vapor deposition (CVD) of $Ru_3(CO)_{12}$, as well as cluster source depositions of bare Ru_3. $TiO_2(100)$ and SiO_2 are used as comparison surfaces with differing cluster-surface interactions. Temperature-dependent X-ray photoelectron spectroscopy (XPS), angle-resolved XPS, and temperature-dependent low energy ion scattering (TD-LEIS) are used to probe how the cluster-surface interaction changes due to heat treatment. Results show that bare Ru_3 supported on SiO_2 remain on the surface layer but agglomerates upon heating. Conversely, when supported on sputter-treated RF-TiO_2, bare Ru_3 is encapsulated by a layer of titania substrate material as-deposited. Ligated $Ru_3(CO)_{12}$ is also covered by a layer of titania when deposited onto sputter-treated RF-TiO_2 but heat treatment is required to remove most of the ligands. TD-LEIS is used to directly measure the encapsulation of CVD $Ru_3(CO)_{12}$ clusters on sputter-treated RF-TiO_2 and determine the substrate overlayer thickness. The overlayer was found to be 1-2 monolayers, which is thin enough for catalytic or photocatalytic reactions to occur without Ru being present in the outermost layer.

Introduction

Small metal clusters are often defined as groups of bound metal atoms with approximately <300 atoms [1-6]. Their electronic and catalytic properties depend on the number of atoms forming the cluster [7]. Ru clusters are of particular interest as they are among the most efficient catalysts for reactions such as CO and CO_2 hydrogenation [8-17]. Two commonly utilised approaches for depositing Ru clusters onto substrates are firstly depositing gas-phase size-selected, bare clusters using a cluster source (CS), and secondly depositing ligand-stabilised clusters such as $Ru_3(CO)_{12}$. The latter can be deposited onto surfaces in two different ways: solution deposition (here shortened to SD, also called solution submersion) [18] and chemical vapor deposition (CVD) [19-29]. The deposition method can affect the resultant cluster properties, however very few studies have directly compared the cluster properties of identically sized clusters resulting from different deposition methods [21, 30].

CS depositions are performed *in situ* and are typically suited for small scale fundamental research studies, while being difficult to upscale for industrial applications due to the high vacuum required and small cluster deposition areas [31-35]. Upscaling, however, is possible with SD and CVD. A secondary advantage of SD is that it allows for cluster deposition within the inner surfaces of porous substrates such as mesoporous silica [36, 37] and zeolites [38, 39], while CS and CVD are line-of-sight depositions. However, SD introduces the possibility of contamination to the samples due to exposure to atmosphere and solvent. Additionally, for both types of ligated cluster depositions (*i.e.* CVD and SD), extra post-deposition surface treatments such as heating or chemical methods are typically used to remove the ligands after deposition to expose bare, surface-supported particles [20, 21, 40, 41].

TiO_2 is a common choice as a substrate for the deposition of clusters [20, 21, 35, 42-53], which is often used due to its photocatalytic activity [54]. Sputtering TiO_2 substrates prior to cluster depositions is a method used to help prevent the agglomeration of clusters [41, 55]; the anchoring of clusters to defect sites on TiO_2 has been demonstrated by experiments [41] as well as DFT calculations [56]. Rutile $TiO_2(110)$ is the most frequently used form of the substrate for fundamental surface science experiments, however here we use RF-deposited TiO_2. This material is prepared by radio frequency (RF) sputtering a TiO_2 wafer over a spinning substrate under high vacuum, which produces a dense, uniform, stoichiometry-controlled layer of TiO_2 which is cheaper and more readily available than $TiO_2(110)$ [57]. RF-TiO_2 has been shown to have a nanoparticulate film structure with spherical-shaped grains distributed across the substrate, with the grain size enlarging upon heat treatment [57-60].

We have previously shown this type of substrate does not feature X-ray diffraction peaks related to a specific crystal phase until modest heating is applied to the substrate under atmosphere or vacuum, upon which an anatase phase is formed and the grain size increases; strong heating under atmosphere to 1373 K for 18 hours also results in a rutile peak emerging in addition to anatase, with no further increase in grain size [58]. Anatase is the most common form used in high surface area catalysis studies.

Clusters deposited on reducible oxides can be strongly affected by the so-called strong metal-support interaction (SMSI), and in some cases may become covered by a layer of support material [43, 61]. This is known as “encapsulation” or “decoration” of the clusters [62, 63]. Depending on the combination of materials for the clusters and substrate, varying conditions have been required to induce cluster encapsulation, including sputtering prior to cluster deposition [43, 44], and high temperature reduction of the cluster/oxide system in ultra-high vacuum (UHV) [42-44, 63-70]. If a sufficient amount of cluster material is present, these changes are typically measurable using X-ray photoelectron spectroscopy (XPS): encapsulation increases the concentration of reduced Ti at the surface which causes a low binding energy (BE) shoulder in the Ti 2p peak [43, 71]. The encapsulation of clusters can potentially reduce their catalytic and/or photocatalytic ability by means of steric hindrance, where reactant molecules are prevented from reaching the clusters [43, 44, 69]. Thus, knowledge about cluster encapsulation is important for catalytic and photocatalytic applications.

There are various analytical techniques which can be used to depth profile systems of small metal clusters. Angle resolved XPS (ARXPS) is commonly used for non-destructive depth profiling [72, 73] but is known to be less reliable for samples which have non-monotonic concentration depth profiles or show significant roughness [73]. Low Energy Ion Scattering (LEIS) allows for measuring the atomic composition of the topmost layer [47, 49, 64, 74-94], and can provide depth information about the atomic distribution over the range 0-10 nm below the surface layer, depending on the ion energy used [95]. It has been shown that cluster encapsulation can be detected by LEIS [64, 74, 87]. For overlayers of a few monolayers (ML), the film thickness can be determined by LEIS as described by Brongersma *et al.* [96], which has previously been applied to determining the overlayer thickness for functionalised Au nanoparticles [97, 98].

In our previous study, CO temperature programmed desorption (CO-TPD) was performed on Ru_3 clusters deposited by CVD ($Ru_3(CO)_{12}$) and CS (bare Ru_3) onto RF-TiO_2 [30]. This involved dosing ^{13}CO onto the samples under UHV, then heating while monitoring the desorbing gas molecules. Because CO binds strongly to Ru but not to the support, this provides a measure of the number of surface-exposed Ru atoms. For the bare CS-Ru_3, substantial CO binding to Ru sites was seen in the first TPD run, but in subsequent runs, the CO signal was much weaker and desorbed at ~200 K lower temperature, *i.e.*, both the number and strength of the Ru-CO binding sites was dramatically reduced, which was attributed to encapsulation of the clusters during the first TPD run. For CS-Ru_3 deposited on sputtered RF-TiO_2, essentially no Ru-CO binding sites were observed even in the first TPD run, suggesting that the sputtered TiO_2 encapsulated the Ru_3 upon deposition. Similarly, no Ru-CO sites were observed for CVD-$Ru_3(CO)_{12}$ clusters deposited on sputtered RF-TiO_2 then heated to drive off the CO ligands prior to the TPD experiments. These results suggested that the Ru_3 clusters became encapsulated by TiO_x, thus blocking the CO sites that would be expected for Ru clusters, however there was no direct evidence for encapsulation. Additionally, XPS measurements of the samples after the CO-TPD experiments indicated that the Ru_3 clusters were partially oxidised by the sputtered RF-TiO_2 substrate after heating to 800 K.

Here, we deposit size-selected Ru_3 clusters onto RF-TiO_2 substrates using 3 different deposition methods: (i) SD, (ii) CVD, and (iii) CS depositions. The first aim was to determine whether the Ru_3 deposition method has any effect on the resultant surface properties before and after heat-treatment. The properties of solution submersion and CVD depositions of the same cluster type have not been previously compared in this way. The second aim was to directly measure the encapsulation of Ru_3 (following on from our previous study) and determine the depth of encapsulation and temperature at which this occurs. Understanding the cluster encapsulation is important for elucidating potential catalytic and photocatalytic benefits of the cluster/substrate system. $TiO_2(110)$ and SiO_2 are also studied for comparison with the RF-TIO_2 substrates; $TiO_2(110)$ is the most commonly used single crystal form of TiO_2 [99], and SiO_2 is chosen as a non-reducible oxide support that does not normally support SMSI or encapsulation [54].

Methodology

Substrates

A list of the substrates used, and their abbreviated names are given in Table 1. RF-TiO_2, TiO_2(110), and SiO_2 were used as substrates for depositions of Ru_3 by solution submersion and CVD of $Ru_3(CO)_{12}$, as well as CS depositions of bare Ru_3. P-type, boron-doped Si (100) wafers were purchased from MTI Corporation and used without further modification. The boron doping makes the wafers conductive and suitable for electron spectroscopy. SiO_2 substrates were prepared by heating to 700 K for 20 minutes under an atmosphere of 7×10^{-6} mbar O_2 to ensure the surface oxide layer, followed by a further 2 minutes of heating under UHV. These substrates are hereafter referred to as SiO_2 due to the fact that they have an amorphous SiO_2 (silica) surface layer [78].

RF-sputter deposited TiO_2 substrates, (RF-TiO_2, also known as RF-deposited TiO_2), were prepared by RF magnetron-sputtering using a 99.9% pure TiO_2 ceramic target onto an SiO_2 wafer. An HHV/Edwards TF500 Sputter Coater was used at a pressure of $<2 \times 10^{-5}$ mbar. This process has been described in detail in previous publications [30, 58]. Based on SEM measurements performed on previously prepared wafers, the thickness of the RF-TiO_2 was approximately 150 nm [58], which is thick enough that the SiO_2 wafer beneath would not affect any measured electron spectra. The nanoparticulate size before heat treatment was shown to be 25-45 nm [58]. RF-TiO_2 was treated prior to cluster depositions by heating to 723 K for 10 minutes, then using 3 different pre-deposition Ar^+ sputtering treatments: namely, NS-RF-TiO_2 (non-sputtered), LDS-RF-TiO_2 (low-dose sputtered, treated with 4×10^{13} Ar^+ ions/cm^2), and HDS-RF-TiO_2 (high dose-sputtered, treated with 6×10^{14} Ar^+ ions/cm^2). Note that LDS-RF-TiO_2 was used only in results presented in the Supplementary Material. An assumption was made (for depth profiling) that the thickness of a ML of RF-TiO_2 could be estimated to be the apical Ti-O bond length of the rutile TiO_2 crystal, 0.198 nm [100].

A 99.99% pure rutile TiO_2(110) single crystal was purchased from MTI Corporation. The sample treatment procedure followed that used in recent publications where TiO_2(110) was used as a substrate for metal clusters [47, 49] and is detailed further in the Supplementary Material (page 2). 6×10^{14} Ar^+ ions/cm^2 was dosed onto the TiO_2(110) prior to cluster depositions.

Table 1: Summary of the different supporting substrates used in this study. The designated sample names and abbreviated names are given.

Substrate Material	Ar^+ Sputter Dose (ions/cm^2)	Designated Sample Name	Abbreviated Name
RF-TiO_2	None	Non-Sputtered RF-TiO_2	NS-RF-TiO_2
RF-TiO_2	4 x 10^{13}	Low-Dose Sputtered RF-TiO_2	LDS-RF-TiO_2
RF-TiO_2	6 x 10^{14}	High-Dose Sputtered RF-TiO_2	HDS-RF-TiO_2
Rutile TiO_2(110) Single Crystal	6 x 10^{14}	TiO_2(110)	TiO_2(110)
SiO_2/Si (100)	None	SiO_2	SiO_2

Instrumentation

Cluster depositions and analysis were performed on 3 separate UHV instruments. *In situ* XPS and LEIS were performed on the University of Utah UHV apparatus and Flinders University UHV apparatus, respectively. ARXPS measurements were performed at the Australian Synchrotron soft X-ray UHV beamline; CVD was performed *in situ* whereas a CS-Ru_3/HDS-RF-TiO_2 sample was prepared at the University of Utah and analysed *ex situ*. All 3 instruments featured their own *in situ* Ar^+ sputtering conditions. At Flinders University and the Australian Synchrotron, experiments used 3 keV sputtering impact energy whereas experiments at the University of Utah used 2 keV. The defects may extend deeper into the bulk for samples prepared with 3 keV impact energy due to the greater impact energy of the Ar^+ [43, 44], however this was not corrected for, with a slight variation in defects on the substrate deemed not to be of critical importance for comparison of the data.

Cluster Depositions

Chemical Vapor Deposition

CVD was performed *in situ* at both Flinders University and the Australian Synchrotron, where $Ru_3(CO)_{12}$ clusters were deposited onto HDS-RF-TiO_2 substrates. CVD-deposited samples are referred to as CVD-$Ru_3(CO)_{12}$. At Flinders University, the CVD procedure followed the method described in the Supplementary Material (page 2), which has also been described in previous work [30]. Briefly, $Ru_3(CO)_{12}$ was inserted into a loading chamber and allowed to evaporate/deposit onto samples; 120 minutes for RF-TiO_2 and 30 minutes for TiO_2(110). At the Australian Synchrotron, the clusters were deposited onto RF-TiO_2 using a modified version of the same procedure, where the $Ru_3(CO)_{12}$ vial was heated to 313 K to increase the deposition rate to a usable level and clusters were deposited for 90 minutes. In all cases, the deposited clusters covered the entire sample area.

Solution Deposition

SD depositions involves submerging a substrate into a solution of the desired clusters into a solvent. $Ru_3(CO)_{12}$ was deposited *ex situ* onto an HDS-RF-TiO_2 substrate by submerging into a 0.2 mM $Ru_3(CO)_{12}$ cluster solution in dichloromethane for 30 minutes. Due to the nature of the deposition procedure this type of deposition cannot be performed under UHV, and the substrate was exposed to atmosphere for approximately 2 minutes before and after submerging. Clusters which were deposited by SD are referred to as SD-$Ru_3(CO)_{12}$. Prior to removing the sample from UHV to perform the solution-based deposition, RF-TiO_2 samples were heated under UHV to 723 K for 10 minutes then Ar^+ sputtered with 6 x 10^{14} ions/cm^2. This procedure coated the whole surface, with an approximately even layer of clusters.

Cluster Source

CS depositions were performed *in situ* by a laser vaporisation CS which has been used in several previous works [30, 75, 76, 78] onto both RF-TiO_2 and SiO_2. The instrument details and standard deposition procedure are given in the Supplementary Material (pages 2-3). RF-TiO_2 substrates with differing sputter dosages were used, as well as SiO_2. Each CS deposition was kept consistent by depositing 1.5 x 10^{14} Ru atoms/cm^2 as mass-selected Ru_3^+, with deposition energy set to ~1 eV/atom to prevent fragmentation of the clusters [101]. Cluster spots were 2 mm in diameter, defined by a mask.

TD-XPS

For TD-XPS measurements, the temperature of a sample is increased in a stepwise manner while XPS is performed at each discrete temperature. Samples are held at each temperature for 10 minutes, then the heating is turned off and XPS is performed as the sample slowly cools. TD-XPS measurements were also performed for substrates with no clusters deposited, which are referred to as “blank samples”. These samples were otherwise treated identically to the cluster-containing SD-$Ru_3(CO)_{12}$/HDS-RF-TiO_2, CVD-$Ru_3(CO)_{12}$/HDS-RF-TiO_2, and CVD-$Ru_3(CO)_{12}$/TiO_2(110) samples. The blank sample for SD on HDS-RF-TiO_2 was submerged in dichloromethane solvent for 30 minutes. The blank samples for CVD on HDS-RF-TiO_2 and CVD on TiO_2(110) were each held in the loading chamber for 5 minutes with no cluster deposition vial present.

TD-XPS of SD-$Ru_3(CO)_{12}$ and CVD-$Ru_3(CO)_{12}$ samples were measured at Flinders University, while CS-Ru_3 samples were measured at the University of Utah. For both instruments, the photons had an incidence angle of 54.7° to the surface and ejected electrons were measured orthogonal to the surface. At Flinders University, a non-monochromatic X-ray source with an Mg anode was used with a Phoibos 100 hemispherical analyser (SPECS, Germany). At The University of Utah, a non-monochromatic X-ray source with an Al anode was used (Physical Electronics); this featured an area-selective lens with a 1.1 mm diameter analysis area, allowing the 2 mm cluster spot to be probed with minimal background from the surrounding cluster-free substrate. For high resolution measurements 10 eV pass energies were used, and each region was averaged over multiple scans. The number of scans per region required for sufficient signal varied depending on the element and surface concentration.

Data Analysis

The program CasaXPS was used to model XPS spectra. Shirley backgrounds[102] were subtracted from each measured spectrum when integrating the fitted peaks. The binding energy (BE) axis was calibrated to C 1s = 285.0 eV for the aliphatic adventitious hydrocarbons on the sample surface. The absolute uncertainty in reported BEs is ± 0.2 eV, however, for comparing BE differences in the same sample before and aftertreatment the uncertainty is reduced to ± 0.1 eV. Information on the peak fitting of C 1s, Ru 3d, and Ti 2p is given in detail in the Supplementary Material (pages 3-6). Based on the XPS peak fitting, atomic concentrations in percentage (At%) were determined and the surface coverage of cluster material was estimated for each cluster deposition. Surface coverages were measured by XPS and are given in terms of percent of a close-packed monolayer (% ML), where one ML is 1.6×10^{15} Ru atoms/cm^2. Further details on these calculations and their uncertainties are given in the Supplementary Material (page 6). The At% and Ru surface coverages for TD-XPS results presented are averages over all measured temperatures for each sample.

ARXPS

ARXPS measurements were performed at the Australian Synchrotron soft X-ray beamline. ARXPS is an extension of the standard XPS protocol which allows a concentration depth profile of the sample to be determined by changing the observation angle of the emitted photoelectrons. For each ARXPS measurement, XPS measurements were taken at observation angles of 0˚, 30˚, 45˚, 55˚, and 60˚, which avoids severe angle effects related to the elastic scattering of photoelectrons by the sample [103]. To determine a depth profile from an ARXPS measurement, a model was made and fitted to the experimental data for a specific At% measured at each observation angle. Two samples were analysed; CVD-$Ru_3(CO)_{12}$/HDS-RF-TiO_2 deposited *in situ*, and CS-Ru_3/HDS-RF-TiO_2 deposited *ex situ* at the University of Utah. Each individual ARXPS measurement was performed at 5 temperatures between room temperature and 723 K for each sample.

The synchrotron X-ray excitation energy used was 720 eV, which was confirmed to not overlap with the peaks of interest. The beamline is equipped with a Phoibos 150 HSA (SPECS, Germany). High resolution spectra were taken at 10 eV pass energy. Further details about the synchrotron X-ray beam and ARXPS data analysis procedure are provided in the Supplementary Material (pages 6-7), including details on the XPS peak fitting and the procedure used to determine concentration depth profiles.

For the CVD-$Ru_3(CO)_{12}$/HDS-RF-TiO_2 sample, it was noticed that synchrotron X-rays partially removes the CO ligands from $Ru_3(CO)_{12}$ clusters. The ligand removal by the beam was further investigated by performing a series of XPS measurements on a single spot at room temperature, shown in the Supplementary Material (pages 21-22). Furthermore, an ARXPS measurement was performed on a cluster spot which was irradiated 3.95×10^{18} photons/cm^2. To avoid beam effects for the main ARXPS measurements, the CVD-$Ru_3(CO)_{12}$/HDS-RF-TiO_2 sample was scanned in a grid such that each angle and temperature measurement was on a virgin area of the sample.

LEIS

Procedure

In LEIS, a sample is bombarded with low energy ions which are backscattered and detected [95, 104]. LEIS is mostly sensitive to the elemental composition of the outermost layer due to the higher neutralisation probability for He^+ projectiles backscattered from layers below the outermost layer [75]. There is, however, a finite probability for backscattering of He^+ projectiles from deeper layers [95]. Further details are given in the Supplementary Material (page 8) on the surface sensitivity of LEIS and the confirmation of the reproducibility of results.

The two LEIS measurement procedures used were “series LEIS” (only reported in the Supplementary Material) and “temperature-dependent LEIS” (TD-LEIS). To avoid damage effects, separate sets of samples were for the LEIS, TD-XPS, and ARXPS experiments. Series LEIS measurements were performed repeatedly in series on the same sample area without further modification, to determine the effects of the He^+ beam on the sample. TD-

LEIS measurements were performed *in situ* on separate samples as the sample temperature was increased to determine the effects of heating. A LEIS measurement was first performed at the deposition temperature. Following this, the He^+ beam was stopped, and the sample was flashed (rapidly heated at 3 K/s) to the next temperature. Heating was stopped as soon as the target temperature was reached, and another LEIS measurement was performed. This process was repeated for regular temperature intervals until 900 K. For each TD-LEIS sample, XPS was performed after the TD-LEIS measurements and used to determine Ru surface coverages.

Instrumentation

In situ LEIS measurements were performed on samples at both Flinders University and the University of Utah, and both LEIS instruments used the same settings. 1 keV He^+ ions were produced using ion guns, which were incident on the sample at 45° and scattered He^+ was detected orthogonal to the sample at a scattering angle of 135°. The backscattered He^+ ions were detected with the same HSA detectors which were used on each UHV apparatus for XPS (see above). Backscattered He^+ counts were plotted against the ratio E/E_0, where E is the backscattered energy and E_0 is the incident ion energy. To minimize damage from He^+ impacts, scan times were kept as low as possible to achieve reasonable resolution, and the He^+ beam was on only during scans. The data analysis procedure is described in detail in the Supplementary Material (page 8). Preliminary testing performed prior to the main TD-LEIS measurements is shown in the Supplementary Material (pages 23-25).

Results and Discussion

TD-XPS

TD-XPS measurements were performed on the 5 samples listed in Table 1. The resulting spectra and analysis are shown in the Supplementary Material (Figures S1-S6). Temperature-dependent results are presented for Ru At%, Ru 3d BE, CO/Ru atomic ratio (for ligated clusters), and the ratio of Ti defects (Ti^{2+} and Ti^{3+}) in the substrate.

It was determined from the Ru 3d BE (Figure S7) that Ru clusters are partially oxidised (see Supplementary Material page 16) due to heating, requiring a temperature of at least 500 K for oxidation to occur on NS-RF-TiO_2 as indicated by a change in BE by +0.2 ± 0.1 eV. This oxidation agrees with XPS results presented in our previous study [30]. The Ru 3d BE was also noticeably affected by the ligand configuration of the clusters at deposition. However, after heat treatment to 723-823 K the Ru 3d BE converged for all TiO_2-supported samples (from 280.5 eV to 280.6 eV), indicating that the Ru_3 clusters have similar oxidation states after heating. For the ligated clusters, the initial CO/Ru ratio (Figure S8) was 2.1 ± ~0.5 for CVD-$Ru_3(CO)_{12}$/HDS-RF-TiO_2, and 1.5 ± ~0.5 for CVD-$Ru_3(CO)_{12}$/TiO_2(110). This implies approximate as-deposited cluster chemical formulae of $Ru_3(CO)_6$ and $Ru_3(CO)_{4.5}$ respectively, meaning some ligands were lost in the CVD procedures. Note that sample SD-$Ru_3(CO)_{12}$ suffered from carbon contamination and its CO/Ru ratio could not be determined (see Supplementary Material page 18).

The density of Ti defects (Figure S9) is shown to generally increase with heating for the ligated $Ru_3(CO)_{12}$/TiO_2 samples. The increase was at least partially due to changes in the substrate. Heating-induced defects for TiO_2 under UHV are well-known and have been reported in previous studies [54, 63, 105]. However, because the sample defects for cluster-loaded samples increased above the level of the blank samples, this suggests the clusters were involved with the increase in surface defects and reducing the surface. Conversely, CS-Ru_3/NS-RF-TiO_2 did not have an increase in Ti defects related to heating. This was unexpected compared to our previous findings [30] because the partial oxidation of the supported CS-Ru_3 as a result of heating would hypothetically increase the number of Ti defects on the surface. It is thus possible that the effect was too small to detect, perhaps due to the lower Ru surface coverage of the CS-Ru_3/NS-RF-TiO_2 compared to CVD-$Ru_3(CO)_{12}$/HDS-RF-TiO_2 (see Table S2).

ARXPS

ARXPS measurements were performed on 2 samples; CVD-$Ru_3(CO)_{12}$/HDS-RF-TiO_2 (deposited *in situ*) and CS-Ru_3/HDS-RF-TiO_2 (deposited *ex situ*). The Ru surface coverage of the ARXPS samples were estimated and are shown in Table 2. The Ru surface coverage for both samples is <5% ML, and thus cluster-cluster interactions were considered negligible, and the samples were directly comparable to one another in terms of Ru properties. The fitted Ru 3d/C 1s region XPS spectra are shown in the Supplementary Material (Figure S10).

Table 2: Ru At% and Ru surface coverages for ARXPS samples. The fitting uncertainty for Ru At% was ~2%. The absolute error in Ru coverage was ~100%, while the relative uncertainty between the experiments was ~2% based on the Ru At%.

Deposition	Substrate	Ru At% (%)	Ru Surface Coverage (% ML)
CVD-$Ru_3(CO)_{12}$	HDS-RF-TiO_2	0.77	4.0
CS-Ru_3	HDS-RF-TiO_2	0.18	1.0

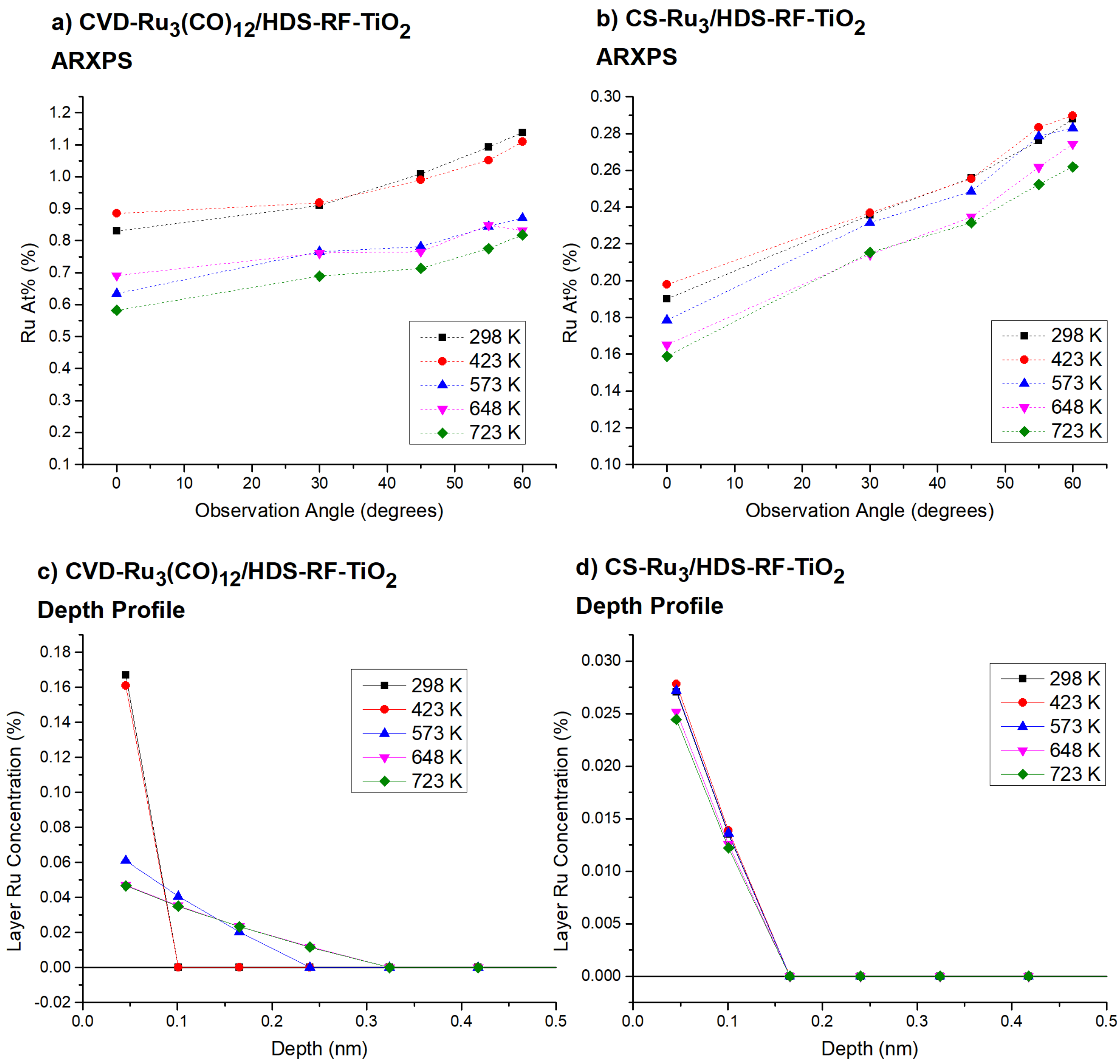

Figure 1: ARXPS data for CVD-$Ru_3(CO)_{12}$/HDS-RF-TiO_2 and CS-Ru_3/HDS-RF-TiO_2. (a) and (b) show the data for Ru At% vs. observation angle for CVD-$Ru_3(CO)_{12}$ and CS-Ru_3, respectively. (c) and (d) show the ARXPS depth profiles for CVD-$Ru_3(CO)_{12}$ and CS-Ru_3, respectively. These show the atomic concentration of Ru per layer for arbitrarily defined layers of the sample, as determined by the ARXPS model. The uncertainty in Ru At% was ± 2%, while the uncertainty in the layer concentration was ± 20%.

The ARXPS results for both CVD-$Ru_3(CO)_{12}$/HDS-RF-TiO_2 and CS-Ru_3/HDS-RF-TiO_2 are shown in Figure 1. Figure 1a and 1b show the measured Ru At% results for CVD-$Ru_3(CO)_{12}$ and CS-Ru_3, respectively. At each temperature, the At% increases with increasing observation angle. This is due to the limited electron mean free path of the electrons emitted from the atoms forming the samples, and thus the Ru clusters which are at the surface or close to the surface have a greater relative signal detected by XPS. These results were used to determine Ru depth profiles for the samples at each temperature (for more details on the data analysis including determining the concentration depth profiles see Supplementary Material, page 7).

Figure 1c shows that the depth profile of CVD-$Ru_3(CO)_{12}$ clusters on the surface change between 423 K and 573 K. Between 298 K and 423 K all Ru was present on the top surface layer. At 573 K the depth profile changes, and clusters either penetrated into deeper layers of the substrate or were covered by an overlayer. The penetration extended deeper again at 648 K to a maximum penetration depth of 0.24 nm ± 0.03 nm, which corresponds in thickness approximately to 1 ML for an overlayer of TiO_2. Based on the ARXPS analysis, the depth profile shows that at 723 K there was approximately 60% Ru below the top-most layer, and 40% present on the surface, based on the relative layer concentrations of Ru.

Figure 1d shows the depth profiles for CS-Ru_3/HDS-RF-TiO_2. The main change observed is a small reduction in the total amount of Ru visible in XPS as the temperature increased. Unlike CVD-$Ru_3(CO)_{12}$, Ru below the top-most layer was present even at 298 K. The ratio of surface to sub-surface Ru was consistent for all temperatures; there was ~66% on the surface and ~34% below the top-most layer. The maximum penetration depth was approximately 0.1 nm ± 0.03 nm, which corresponds to approximately 0.5 ML for an overlayer of TiO_2. The calculated value being <1 ML may suggest that not all the clusters were covered, or that the cluster are only partially covered by the substrate. However, comparison to previous results [30] suggests the clusters were indeed fully covered by the substrate. The nature of the overlayer for both samples is discussed in further detail in the Encapsulation section below.

TD-LEIS

TD-LEIS measurements were performed on CS-Ru_3/SiO_2 (Figure 2) and CVD-$Ru_3(CO)_{12}$/HDS-RF-TiO_2 (Figure 3). For the latter, two identical samples were prepared and analysed (referred to as TD-LEIS A and TD-LEIS B). Measurements were also performed on CS-Ru_3 on RF-TiO_2 with 3 different pre-deposition sputtering doses, but Ru peaks were obscured in the LEIS results, most likely by carbonaceous contamination (results shown and discussed in Supplementary Material, pages 26-29, Figures S15-16).

(A) Ru Surface Coverage and Ion Dosage

XPS was performed on each of the TD-LEIS samples after the TD-LEIS measurements were completed to estimate Ru surface coverage in order estimate potential damage induced during the LEIS measurements. These XPS results are given in Table 3. The ratio of total carbon atoms to Ru atoms was calculated and provides a measure of the level of contamination on each sample. In addition, the total ion dose for each measurement is shown, along with the estimated percentage of Ru removed by the He^+ which was used as a measurement for the level of Ru cluster removal due to LEIS (see Supplementary Material pages 8-9 for further details). Between all TD-LEIS samples, the percentage of Ru sputtered from the surface during a measurement was an average of 2.9%, and a maximum of 6.8%. These values were cumulative over the TD-LEIS measurements at all temperatures, and this level of cluster removal was small enough that He^+ beam effects were neglected as a justification for any changes to Ru peaks in TD-LEIS spectra.

Table 3: Ru At%, Ru surface coverage, C/Ru ratio, total He^+ dose, and total removed Ru for all TD-LEIS samples. Measurements were after TD-LEIS, and the samples were heated to 900 K. An example calculation for Ru removal by the beam was given in the Supplementary Material (pages 8-9).

Deposition	Substrate	Ru At% (%)	Ru Surface Coverage (% ML)	C/Ru Atomic Ratio	Total Ion Dose (ions/cm^2)	Total Ru Removed (%)
CS-Ru_3	SiO_2	0.5	3.3	5.4	1.2×10^{15}	1.3
CVD-$Ru_3(CO)_{12}$	HDS-RF-TiO_2	1.5	10.7	1.5	6.0×10^{15}	6.8

(B) CS-Ru_3/SiO_2

The lowest and highest temperature LEIS spectra for the TD-LEIS of CS-Ru_3/SiO_2 are shown in Figure 2a, with peaks labelled for Ru, Si, and O. The spectra were integrated, and the peak ratio of Ru/(Si+O) was determined at each temperature. This forms the core TD-LEIS result, and is shown in Figure 2b.

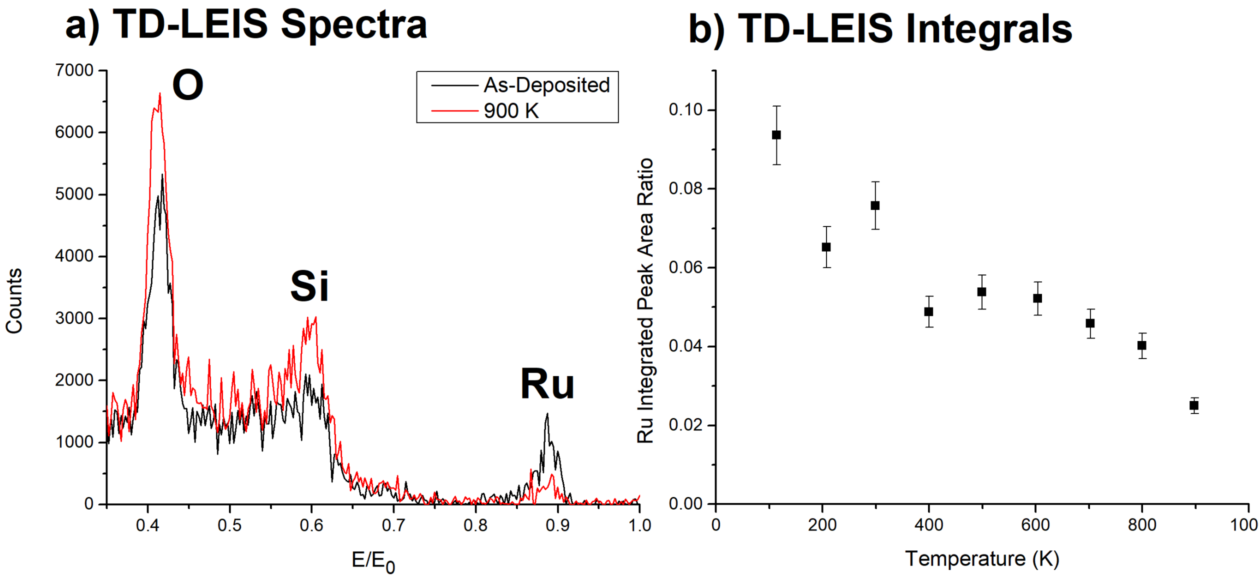

Figure 2: TD-LEIS of CS-Ru$_3$/SiO$_2$. a) LEIS spectra for initial and final temperature measurements. b) integrated Ru/(Si+O) peak ratio vs. temperature. Uncertainties in the Ru peak area ratios were ~8%. The sputter effects of the He$^+$ on the sample are discussed in the Supplementary Material (see Figure S14).

In Figure 2a the intensities of the LEIS peaks from the SiO$_2$ support increase after heating to 900 K, indicating that the fraction of clean substrate increased, attributed to some combination of desorption of adventitious adsorbates and reduction of the fraction of the surface area blocked or shadowed by Ru clusters. Conversely, the Ru peak intensity decreased monotonically with increasing temperature, such that the Ru/(Si+O) intensity ratio (Figure 2b) dropped by a factor of ~3 from 300 to 900 K. Such a decrease could indicate that the clusters become partially covered by some adsorbate, or that the clusters sintered into multi-layer structures where some of the Ru atoms are no longer in the LEIS-accessible surface layer. In this case, the decrease in Ru intensity begins at quite low temperature, where SiO$_2$ should be stable, and in a temperature range where adventitious adsorbates would have been desorbing, and thus the conclusion is that the Ru$_3$ clusters sintered significantly. This conclusion is consistent with previous studies which found that Pt$_n$ clusters [77, 81] and Ir$_n$ clusters [106] deposited on SiO$_2$ undergo sintering when heated over this temperature range, giving rise to similar changes in LEIS signals. The agglomeration of Ru clusters on SiO$_2$ was also supported by our previous study [30] examining CO-TPD, where the change in the CS-Ru$_3$/SiO$_2$ CO-TPD spectra with repeated heating cycles provided evidence the clusters were agglomerated when heated to 800 K.

(C) CVD-$Ru_3(CO)_{12}$/HDS-RF-TiO_2

A TD-LEIS measurement of CVD-$Ru_3(CO)_{12}$/HDS-RF-TiO_2 was performed two times using separate samples, referred to as TD-LEIS A and TD-LEIS B. Figure 3 shows the measured TD-LEIS spectra for one of these measurements (TD-LEIS A), and the analysed data for both measurements.

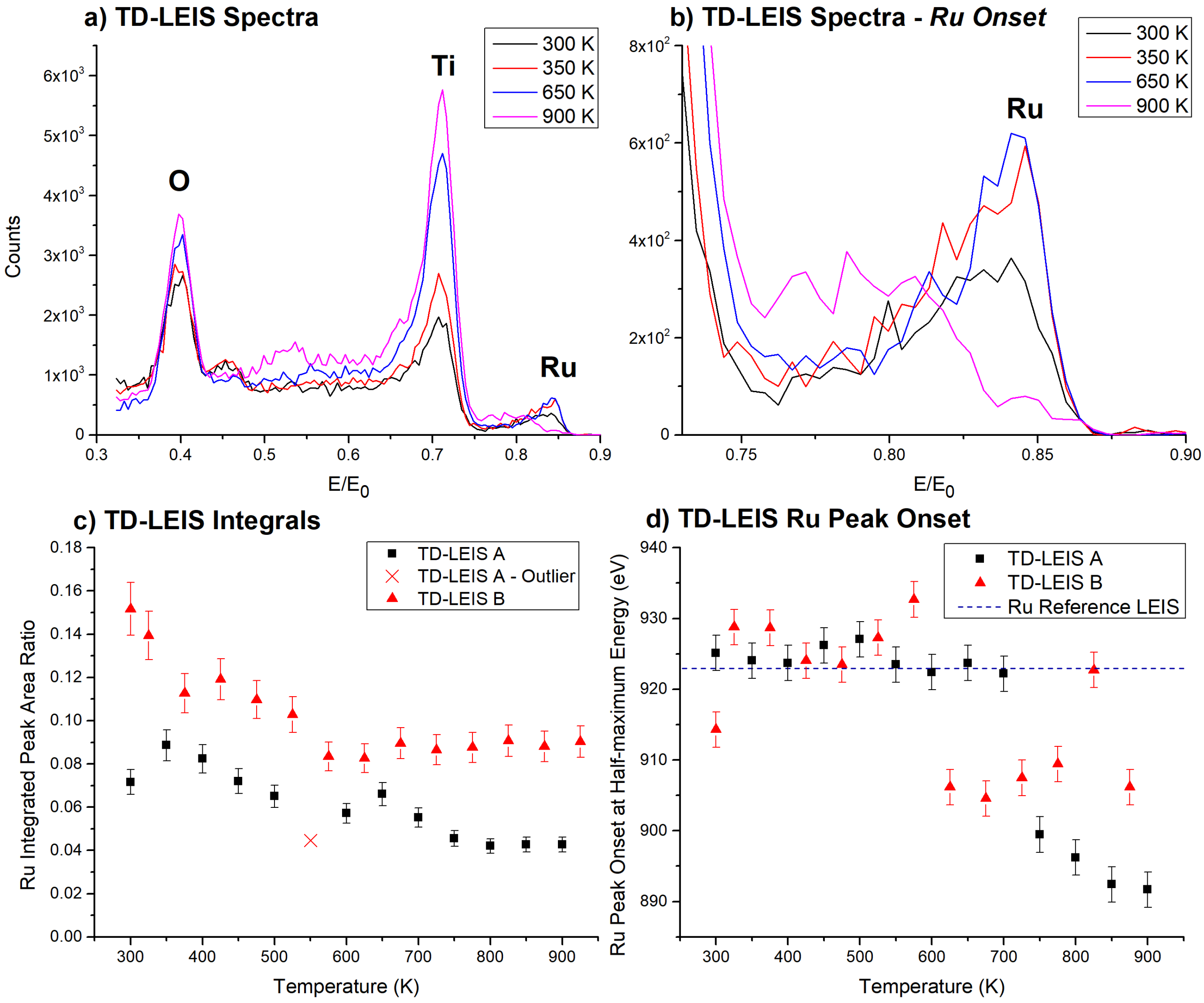

Figure 3: TD-LEIS of CVD-$Ru_3(CO)_{12}$/HDS-RF-TiO_2. Separate depositions and TD-LEIS measurements were performed on 2 samples. (a) and (b) show spectra from TD-LEIS A, while (c) and (d) show collated data from both TD-LEIS measurements. a) LEIS spectra at selected temperatures. b) LEIS spectra at selected temperatures, zoomed in to the Ru peak region. c) Integrated Ru/(Ti+O) peak ratios vs. temperature. Data point × was included for completion but was treated as an outlier. Uncertainties in Ru integrated peak ratios were ~8%. d) Half-maximum peak onset for Ru vs. temperature, in terms of backscattered He^+ energy. The black dashed line at 923 eV represents the Ru half-maximum onset for a metallic Ru reference sample. The error bars were ± 2.5 eV based on the bin width.

Figure 3a shows LEIS spectra at all temperatures measured for CVD-$Ru_3(CO)_{12}$/HDS-RF-TiO_2. The overall signal strength increased with increasing temperature, which is indicative of surface contamination being desorbed and sputtered away by the He^+ beam, with the contamination most likely being adventitious hydrocarbons. Figure 3b displays the Ru peak region. The onset slope of the Ru peak (on the right) decreased at 650-700 K, and decreased further as the temperature was increased to 850 K. The shape then remained constant when heated to 900 K. Starting at 650-700 K, the counts at ~0.79 E/E_0 increased while the main peak at ~0.85 decreased in size, shifting the peak location of Ru to lower E/E_0 values. In LEIS, peaks shifting to lower E/E_0 values in cases such as this can be indicative of the clusters being covered by a material overlayer which the He^+ needs to penetrate through before and after backscattering. In such cases the He^+ projectiles lose energy due to penetrating through the overlayer, which shifts the peak to lower values of E/E_0[98, 104]. Backscattered projectiles have a finite probability of re-ionisation when leaving the surface which results in a measurable signal of backscattered He^+. [98, 104] The TD-LEIS results are supported further by evidence from our previous study [30], where it was proposed based on CO-TPD results that CVD-$Ru_3(CO)_{12}$/HDS-RF-TiO_2 may be encapsulated by the HDS-RF-TiO_2 substrate when heated, based on the loss of all Ru-CO binding sites after heating the sample to 723 K. This aligns with the evidence of an overlayer presented by the TD-LEIS and ARXPS results, and together they present a strong argument that the clusters were encapsulated by the RF-sputtered TiO_2 substrate. This is discussed in detail in the Encapsulation section below.

In Figure 3c the integrated Ru peak ratios are shown vs. temperature, where the integration included both the high and low energy regions of the Ru peak (for surface and sub-surface species). The relative Ru LEIS peak size decreased with increasing temperature. The decrease in intensity is most likely due to the encapsulation of the clusters, which aligns with the ARXPS results, the evidence from Figure 3c where the LEIS peak shifted to lower values [98, 104], and our previous CO-TPD results [30]. This is possibly combined with some amount of Ru sputtering by the He^+ beam. Two LEIS measurements (A and B) show similar trends of decreasing integrated Ru intensity and shift in onset energies although TD-LEIS B has a higher Ru/(Ti+O) ratio at all temperatures. The intensity differences are due to TD-LEIS B having a higher background count rate, which was not subtracted for the peak integrations. The data point marked with a × had a lower ratio than expected because the sample was left in the vacuum chamber after heating due to an equipment issue, which allowed some adventitious hydrocarbons to adsorb atop the clusters.

Figure 3d shows the onset half-maximum energy determined from the high E/E_0 side of the Ru peaks in each TD-LEIS spectrum. This is the energy where the Ru peak reached half its maximum height. For TD-LEIS A, the energy for the onset of the half-maximum is approximately the same as the metallic Ru value (indicated by the black dotted line) until heating to 750 K, where the energy for the onset of the half-maximum shifted to a lower energy. After 750 K the energy for the onset of the half-maximum decreased slightly further due to heating to 900 K. For TD-LEIS B, the shift to a lower Ru energy for the onset of the half-maximum occurred at 575 K and was otherwise the same as TD-LEIS A within the experimental uncertainty. The large shift in the energy for the onset of the half-maximum observed for both measurements corresponds to the complete loss of the surface peak and is treated as an indicator of the clusters being covered by a substrate overlayer.

The shift in the energy for the onset of the half-maximum of the Ru contribution in LEIS as shown in Figure 3d allows for determining the thickness of the titania layer covering the clusters for the CVD-$Ru_3(CO)_{12}$/HDS-RF-TiO_2 sample after heating. A similar method was used in studies by Belsey *et al*. [98] and Hoffman *et al.* [107], where in both cases Au nanoparticles were covered with an organic layer. For each TD-LEIS measurement (A and B), the onset half-maximum energies were averaged before and after the onset temperature for penetration into the substrate, and the shift between these was calculated to determine the loss of He^+ energy due to the stopping power of the overlayer, ΔE (this did not include the backscattering energy loss). ΔE was determined to be 29.9 eV ± 5.3 eV and 19.7 eV ± 5.2 eV for TD-LEIS A and B, respectively, with an average value of 24.8 eV ± 5.3 eV.

To determine the thickness of the TiO_2 layer, ΔE was divided by the stopping power of the overlayer to give the total length of titania which the He^+ projectiles travelled through, L. The beam impact angle (45°) and the angle to the detector (90°) were incorporated using a scaling factor based on right-angle trigonometry to determine the titania depth D. This relationship is shown in Equation 1.

$$D = 0.414\,\mathrm{L} = \frac{0.414\,\Delta E}{Stopping\ Power} \qquad \mathbf{1}$$

The software package Stopping and Range of Ions in Matter (SRIM) was used to calculate the stopping power of He^+ ions in TiO_2; 30 ± 3 eV/nm (see Supplementary Material, page 8 for further details). This calculation uses Bragg's rule [108], and thus any effect of the specific structure of RF-TiO_2 on the stopping power was neglected. Based on equation 1, it was determined that the average D = 0.35 nm ± 0.08 nm, which is approximately 1.7 ML of TiO_2.

The results are the same as ARXPS within experimental uncertainty. The TD-LEIS results are considered to be more reliable than the AXPS results for overlayer depth because LEIS is known for its extreme surface sensitivity [75] while ARXPS is considered to be unreliable for non-monotonic concentration depth profile [73]. The results are comparable to previously reported results in a study by Fu *et al.* [71], where 3 samples of Pd nanoparticles on $TiO_2(110)$ were analysed using the shift in the Rutherford backscattering high energy edges of Pd and found to have TiO_x overlayers with thicknesses of 0.13 nm, 0.14 nm, and 0.27 nm.

Encapsulation

The results reported herein provide evidence for an encapsulation reaction occurring between deposited Ru clusters and RF-TiO_2. It is often proposed that for encapsulation to occur there must be a thermodynamic advantage which is given by the tendency of a system to minimize the total surface energy of the system. To drive encapsulation, the surface energy of the metal adsorbate must be greater than the surface energy of the supporting layer [43, 63, 66, 67, 69, 71]. The combination of Ru clusters and TiO_2 substrate fits this condition; the surface energy of Ru is 3.409 J/m^2 [109] and $TiO_2(110)$ is 1.78 J/m^2 [110, 111].

The ARXPS results in Figure 1c provide evidence that $Ru_3(CO)_{12}$/HDS-RF-TiO_2 is covered by an overlayer following heating. This was supported by the TD-LEIS results in Figure 3 which measured the depth of the overlayer after heating. Further comparison to our previous study [30] provides strong evidence that this is due to cluster encapsulation by the substrate. In our previous study, CO-TPD results showed that CVD-$Ru_3(CO)_{12}$/HDS-RF-TiO_2 had no Ru-CO binding sites remaining after heating to 800 K indicating that no Ru was exposed on the surface layers. This is consistent with the presence of an overlayer encapsulating the clusters.

Regarding CS-deposited clusters, in our previous experiment [30] the as-deposited CS-Ru_3/HDS-RF-TiO_2 did not have any Ru-CO binding sites present on the surface layer before or after heat treatment. This aligns with the ARXPS results in Figure 1d, showing there is sub-surface Ru present as-deposited (which did not change due to heat treatment). These results suggest that the clusters in this sample are encapsulated as-deposited without heat treatment (while heat treatment was required for encapsulation in CVD-$Ru_3(CO)_{12}$-HDS-RF-TiO_2). Conversely, there was no evidence for cluster encapsulation or overlayers occurring for the CS-Ru_3/SiO_2 sample before or after heat treatment. However, there was in this case evidence that the clusters sinter upon heat treatment (see Figure 2). A summary of the encapsulation results is given in Table 4.

Table 4: Summary of the Ru_3 cluster encapsulation results for the samples analysed using ARXPS and/or TD-LEIS. The state of the clusters is given as-deposited, and after heat treatment to 723 K or 900 K (see text for details).

Sample	As-Deposited	After Heat Treatment
CVD-$Ru_3(CO)_{12}$/HDS-RF-TiO_2	Clusters on top-most layer	Encapsulated clusters
CS-Ru_3/HDS-RF-TiO_2	Encapsulated clusters	Encapsulated clusters
CS-Ru_3/SiO_2	Clusters on top-most layer	Agglomerated clusters, with no encapsulation

There is an apparent inconsistency between the ARXPS results and both the TD-LEIS results and CO-TPD results from our previous study [30]. The ARXPS results (Figure 1c-d) suggest that some Ru was still present on the topmost layer for both the CVD-Ru_3/HDS-RF-TiO_2 and CS-Ru_3/HDS-RF-TiO_2 samples, even after heating. However, the CO-TPD results, as well as the TD-LEIS results for CVD-$Ru_3(CO)_{12}$-HDS-RF-TiO_2, both suggest there is no Ru on the surface layer. This discrepancy is simply attributed to the limitation of the depth analysis by ARXPS. Analysis of the differences in the At% determined experimentally and in the ARXPS model supports this (see Supplementary Material, Figure S12), indicating that there may have been effects related to the roughness or non-monotonic nature of the sputtered RF-TiO_2 substrates on the ARXPS results. Based on this, the ARXPS depth profiles are treated as less quantitative regarding the composition of the outermost layer than TPD and LEIS.

The encapsulation of unheated CS-Ru_3/HDS-RF-TiO_2 was not expected, because conditions typically reported to induce encapsulation involve high temperature heating of the oxide substrate under UHV [42-44, 63-70, 110] or exposure to H_2 [61, 62, 112-114]. As cluster-specific examples, Ovari *et al.* [74] used LEIS to show that Rh clusters were present on a $TiO_2(110)$ surface layer until 700 K, however after heating to 900 K the clusters were encapsulated. Similarly, in another example for Pd clusters on $TiO_2(110)$ the encapsulation started at ~553 K, where the authors suggested that the activation of defect mobility due to heating was required for encapsulation to occur [43]. Because no heating was required for the encapsulation of CS-Ru_3 by sputtered RF-TiO_2, this implies a different encapsulation mechanism which is not based on heat-activated defect mobility. Defect mobility without heating is also not likely, as defect mobility is typically only shown at elevated temperatures [43, 54, 115]. It is possible that the mechanism for encapsulation is that the reactivity of the titania surface is increased due to sputter-induced defects, which easily interact with the Ru_3 without heat-treatment. Subsurface Ti defects may also be responsible for attracting the clusters below the surface. Similarly, subsurface oxygen may be more readily available for the Ru_3 than surface oxygen and attract the clusters below the surface. However, the exact mechanism for encapsulation cannot be determined from the TD-LEIS and ARXPS results. Additionally, results are not provided about the structure of the CS-Ru clusters underneath the overlayers.

To our knowledge, this type of titania encapsulation of small Ru clusters has not been previously reported in the literature, although some encapsulation studies using larger Ru materials have been conducted [116, 117]. In fact, there is a previous measurement by Zhao *et al.* of $Ru_3(CO)_{12}$ supported on $TiO_2(110)$ where the surface was heat treated under UHV and encapsulation did not occur, as evidenced by the availability of Ru-CO binding sites [20]. The differences between this study and other literature can be attributed to the differences between the titania substrates; $TiO_2(110)$ was used in the referenced cluster encapsulation studies [43, 74], which does not have the same surface properties as the HDS-RF-TiO_2 used in this study. That encapsulation varies with cluster/substrate system is well known in the literature [42, 43, 66, 118, 119].

The TD-XPS results for the encapsulated cluster sample CVD-$Ru_3(CO)_{12}$/HDS-RF-TiO_2 showed an increase in Ti defect ratio beyond the blank sample (Figure S9). In the literature, increased Ti defects for substrates loaded with clusters has previously been associated with clusters being encapsulated by reduced titania for other TiO_2-supported systems, including Pd/TiO_2 [43, 69], Pt/TiO_2 [63, 66], and Rh/TiO_2 [44, 67, 68]. This aligns with the encapsulation evidence from ARXPS and TD-LEIS in this study, suggesting that the overlayer was most likely composed of reduced titania, *i.e.* TiO_x, where $x < 2$.

For CVD-$Ru_3(CO)_{12}$/HDS-RF-TiO_2, both the de-ligation of CO and encapsulation of the clusters occurred when the samples were heated. This naturally raises a question about how the ligand removal is related to cluster encapsulation. In the TD-XPS results, CO/Ru atomic ratios indicated most CO ligands were removed by heating to 423 K (Figure S8), but there may have still been one or a few ligands attached until higher temperatures are reached. In the synchrotron ARXPS depth profile (Figure 1c), the clusters were all on the surface layer at 423 K but encapsulation began upon heating to 523 K and reached the full depth at 648 K. TD-LEIS similarly showed encapsulation was completed (*i.e.* no Ru in the surface layer) at 660 K ± 120 K. Because ARXPS showed encapsulation did not start until 523 K, it is concluded that most of the ligands need to be removed for encapsulation but that complete ligand removal is not required. Therefore, there is no existing temperature range where completely bare Ru clusters can exist on the surface layer without encapsulation. This outcome must be kept in mind when considering catalytic applications, because it is often desired to remove the ligands to expose bare clusters for catalysis [20, 21, 40, 41].

Application for Catalysis

For catalytic applications, encapsulation of supported metal catalysts by the substrate material is generally not desirable because the catalytic properties can be affected by either the change in properties of the metal, or the steric hindrance of reactant molecules being blocked from the metal catalyst [43, 44, 69]. However, if the covering layer is thin enough some combinations of clusters and covering layer can yield an electronic structure which is suitable for catalysis and/or photocatalysis without direct reactant-cluster contact [120-122]. This combination can also be considered as a form of doping, and in these cases there can be benefits such as increasing resistance to cluster agglomeration [120, 121], increasing reaction selectivity [122], or improving activity by hindering back reactions which remove reaction products [121]. As an example, the water splitting photocatalytic activity of $Au_{25}/BaLa_4Ti_4O_{15}$ was increased 19-fold due to cluster encapsulation by 0.8-0.9 nm thick Cr_2O_3. This system had a dual benefit for catalysis of decreasing the rate of the O_2 photoreduction back-reaction, as well as decreasing the level of UV irradiation-induced cluster agglomeration which occurred [121, 123]. Using HRTEM imaging, Negishi and co-workers showed that the clusters were ~1 nm in diameter with a Cr_2O_3 overlayer 0.8-0.9 nm thick [121].

Considering these previous findings, the effect of the titania overlayer on the catalytic and photocatalytic activity of the Ru clusters must be tested explicitly for reactions such as catalytic CO hydrogenation and photocatalytic water splitting to determine their viability. There is potential for the titania overlayer to increase the stability of the clusters without suppressing the catalytic reaction. The estimated overlayer depth in the study by Negishi [121] was ~3 times thicker than the 0.35 nm ± 0.08 nm overlayer depth for Ru found in this study, suggesting that the Ru clusters may still be somewhat reactive. Given the catalytic potential for supported Ru clusters [8-17], these encapsulated Ru clusters are a strong candidate for future studies on encapsulated catalysts. Furthermore, in a future study the catalytic and/or photocatalytic activity of supported Ru clusters could be compared between ligated clusters (below ~423 K) and the de-ligated, encapsulated clusters (complete encapsulation occurs at ~648-660 K). Such a course of work is warranted as catalytic effects have been shown in some cases for ligated clusters even if ligands are still attached [124].

Conclusions

Ru_3 clusters were deposited by both solution-based and CVD depositions of $Ru_3(CO)_{12}$, as well as CS depositions of bare Ru_3 onto SiO_2 and a variety of TiO_2 substrates. The TD-LEIS results provide evidence that CS-Ru_3 clusters agglomerate due to heat treatment when supported on SiO_2. TD-XPS showed that the oxidation state of Ru on TiO_2 varied for as-deposited clusters depending on the deposition method and type of TiO_2 substrate (RF-TiO_2 or TiO_2(110)). After heat treating to 723-873 K, the oxidation states for Ru become identical, within experimental accuracy, for all the analysed TiO_2 systems including RF-TiO_2 and TiO_2(110). The results suggest that for catalytic purposes, the specific deposition process is probably not of importance if the clusters are to be heated.

TD-LEIS results provided a direct measurement for the encapsulation of CVD-deposited Ru_3 by a layer of substrate material when supported on sputtered RF-TiO_2, showing that no Ru was left on the topmost layer after heat treatment to 660 K ± 120 K. The overlayer thickness was measured by TD-LEIS to be 0.35 nm ± 0.08 nm for CVD-$Ru_3(CO)_{12}$/HDS-RF-TiO_2, equivalent to an average of 1.74 ML ± 0.41 ML of titania. ARXPS showed encapsulation starting between 423-573 K, reaching a maximum by 648 K. Combined with the TD-XPS results, this suggests that most of the CO ligands need to be removed for encapsulation and that complete de-ligation is not required. ARXPS provided evidence that bare CS-Ru_3 on HDS-RF-TiO_2 was encapsulated as-deposited. Cluster encapsulation may provide an advantage for catalysis or photocatalysis applications by modifying the cluster properties, based on recent studies [121].

Supplementary Material

The supplementary material provides detailed descriptions of the instruments and the experimental techniques applied. The raw data for the C 1s/Ru 3d and Ti 2p regions, and the TD-XPS and LEIS data are also shown.

Acknowledgements

The work is supported by the US army project FA5209-16-R-0017. Part of the work is supported by the Australian Solar Thermal Research Institute (ASTRI), a project supported by the Australian Government, through the Australian Renewable Energy Agency (ARENA). The work at the University of Utah was partly supported by the Air Force Office of Scientific Research, under AFOSR grant FA9550-19-1-0261. The authors acknowledge the facilities, and the scientific and technical assistance, of Microscopy Australia (formerly known as

AMMRF) and the Australian National Fabrication Facility (ANFF) at Flinders University. The authors acknowledge Flinders Microscopy and Microanalysis and their expertise. The authors acknowledge the support from the Australian Synchrotron (grant M15819) and the support of Dr Bruce Cowie from the Australian Synchrotron.

Data Availability Statement

The data that support the findings of this study are available from the corresponding author upon reasonable request.

References

[1] D. Lee, R.L. Donkers, G. Wang, A.S. Harper, R.W. Murray, Electrochemistry and optical absorbance and luminescence of molecule-like Au38 nanoparticles, J. Am. Chem. Soc. 126 (2004) 6193-6199.
[2] J. Jung, H. Kim, Y.-K. Han, Can an electron-shell closing model explain the structure and stability of ligand-stabilized metal clusters?, J. Am. Chem. Soc. 133 (2011) 6090-6095.
[3] G. Ramakrishna, O. Varnavski, J. Kim, D. Lee, T. Goodson, Quantum-sized gold clusters as efficient two-photon absorbers, J. Am. Chem. Soc. 130 (2008) 5032-5033.
[4] M. Valden, X. Lai, D.W. Goodman, Onset of catalytic activity of gold clusters on titania with the appearance of nonmetallic properties, Science 281 (1998) 1647-1650.
[5] C. Xu, X. Lai, G. Zajac, D. Goodman, Scanning tunneling microscopy studies of the TiO2 (110) surface: structure and the nucleation growth of Pd, Phys. Rev. B 56 (1997) 13464.
[6] C.P. Joshi, M.S. Bootharaju, O.M. Bakr, Tuning properties in silver clusters, J. Phys. Chem. Lett. 6 (2015) 3023-3035.
[7] A. Sanchez, S. Abbet, U. Heiz, W.D. Schneider, H. Hakkinen, R.N. Barnett, U. Landman, When gold is not noble: nanoscale gold catalysts, J. Phys. Chem. A 103 (1999) 9573.
[8] C. Moreno-Castilla, M.A. Salas-Peregrín, F.J. López-Garzón, Hydrogenation of carbon oxides by Ru/activated carbon catalysts obtained from Ru3(CO)12: effect of pretreatment on their dispersion, composition and activity, J. Mol. Catal. A: Chem. 95 (1995) 223-233.
[9] P. Panagiotopoulou, Hydrogenation of CO2 over supported noble metal catalysts, Appl. Catal. A 542 (2017) 63-70.
[10] R. Mutschler, E. Moioli, A. Züttel, Modelling the CO2 hydrogenation reaction over Co, Ni and Ru/Al2O3, J. Catal. 375 (2019) 193-201.
[11] G.D. Weatherbee, C.H. Bartholomew, Hydrogenation of CO2 on group VIII metals: IV. Specific activities and selectivities of silica-supported Co, Fe, and Ru, J. Catal. 87 (1984) 352-362.
[12] K. Asakura, Y. Iwasawa, Surface structure and catalysis for CO hydrogenation of the supported Ru species derived from the Ru3(CO)12 inorganic oxides, J. Chem. Soc., Faraday Trans. 86 (1990) 2657-2662.
[13] F. Solymosi, A. Erdöhelyi, M. Kocsis, Methanation of CO2 on supported Ru catalysts, J. Chem. Soc., Faraday Trans. 1 77 (1981) 1003-1012.
[14] W.R. Hastings, C.J. Cameron, M.J. Thomas, M.C. Baird, Carbon monoxide and carbon dioxide hydrogenation catalyzed by supported ruthenium carbonyl clusters. A novel procedure for encapsulating triruthenium dodecacarbonyl within the pores of Na-Y zeolite, Inorganic Chemistry 27 (1988) 3024-3028.
[15] C.S. Kellner, A.T. Bell, Effects of dispersion on the activity and selectivity of alumina-supported ruthenium catalysts for carbon monoxide hydrogenation, J. Catal. 75 (1982) 251-261.
[16] R.D. Gonzalez, H. Miura, Methanation and Fischer-Tropsch studies on potassium-promoted silica-supported Ru catalysts, J. Catal. 77 (1982) 338-347.
[17] E. Kikuchi, H. Nomura, M. Matsumoto, Y. Morita, Fischer-tropsch synthesis of hydrocarbons on V2O3-supported ruthenium catalysts, Appl. Catal. 7 (1983) 1-9.
[18] K. Asakura, K.-K. Bando, Y. Iwasawa, Structure and behaviour of Ru3(CO)12 supported on

inorganic oxide surfaces, studied by EXAFS, infrared spectroscopy and temperature-programmed decomposition, J. Chem. Soc., Faraday Trans. 86 (1990) 2645-2655.

[19] G.A. Rizzi, A. Magrin, G. Granozzi, Substitutional Ti(1-x)RuxO2 surface alloys obtained from the decomposition of Ru3(CO)12 on TiO2 (110), Phys. Chem. Chem. Phys. 1 (1999) 709-711.

[20] X. Zhao, J. Hrbek, J.A. Rodriguez, The decomposition and chemistry of Ru3(CO)12 on TiO2 (110) studied with X-ray photoelectron spectroscopy and temperature programmed desorption, Surf. Sci. 575 (2005) 115-124.

[21] D. Meier, G. Rizzi, G. Granozzi, X. Lai, D. Goodman, Ru3(CO)12 adsorption and decomposition on TiO2, Langmuir 18 (2002) 698-705.

[22] T. Cai, Z. Song, Z. Chang, G. Liu, J. Rodriguez, J. Hrbek, Ru nanoclusters prepared by Ru3(CO)12 deposition on Au (111), Surf. Sci. 538 (2003) 76-88.

[23] F. Yang, S. Kundu, A.B. Vidal, J. Graciani, P.J. Ramírez, S.D. Senanayake, D. Stacchiola, J. Evans, P. Liu, J.F. Sanz, Determining the Behavior of RuOx Nanoparticles in Mixed-Metal Oxides: Structural and Catalytic Properties of RuO2/TiO2 (110) Surfaces, Angew. Chem. Int. Ed. 50 (2011) 10198-10202.

[24] P. Serp, P. Kalck, R. Feurer, Chemical vapor deposition methods for the controlled preparation of supported catalytic materials, Chem. Rev. 102 (2002) 3085-3128.

[25] J.A. Rodriguez, J. Dvorak, T. Jirsak, J. Hrbek, Formation of Mo and MoSx nanoparticles on Au (111) from Mo(CO)6 and S2 precursors: electronic and chemical properties, Surf. Sci. 490 (2001) 315-326.

[26] R. Psaro, S. Recchia, Supported metals derived from organometallics, Catal. Today 41 (1998) 139-147.

[27] M. Xu, F. Zaera, Mechanistic studies of the thermal decomposition of metal carbonyls on Ni (100) surfaces in connection with chemical vapor deposition processes, Journal of Vacuum Science & Technology A: Vacuum, Surfaces, and Films 14 (1996) 415-424.

[28] A.C. Papageorgiou, K. Diller, S. Fischer, F. Allegretti, F. Klappenberger, S.C. Oh, O.z. Sağlam, J. Reichert, A. Wiengarten, K. Seufert, In Vacuo Porphyrin Metalation on Ag(111) via Chemical Vapor Deposition of Ru3(CO)12: Mechanistic Insights, J. Phys. Chem. C 120 (2016) 8751-8758.

[29] E. Mohimi, Z.V. Zhang, S. Liu, J.L. Mallek, G.S. Girolami, J.R. Abelson, Area selective CVD of metallic films from molybdenum, iron, and ruthenium carbonyl precursors: Use of ammonia to inhibit nucleation on oxide surfaces, J. Vac. Sci. Technol. A 36 (2018) 041507.

[30] L. Howard-Fabretto, T.J. Gorey, G. Li, S. Tesana, G.F. Metha, S.L. Anderson, G.G. Andersson, The interaction of size-selected Ru3 clusters with RF-deposited TiO2: probing Ru-CO binding sites with CO-Temperature Programmed Desorption, Nanoscale Advances (2021).

[31] G.E. Johnson, R. Colby, J. Laskin, Soft landing of bare nanoparticles with controlled size, composition, and morphology, Nanoscale 7 (2015) 3491-3503.

[32] T. Choudhary, C. Sivadinarayana, C.C. Chusuei, A. Datye, J. Fackler Jr, D. Goodman, CO oxidation on supported nano-Au catalysts synthesized from a [Au6(PPh3)6](BF4)2 complex, J. Catal. 207 (2002) 247-255.

[33] H.S. Al Qahtani, R. Higuchi, T. Sasaki, J.F. Alvino, G.F. Metha, V.B. Golovko, R. Adnan, G.G. Andersson, T. Nakayama, Grouping and aggregation of ligand protected Au9 clusters on TiO2 nanosheets, RSC Adv. 6 (2016) 110765-110774.

[34] G.G. Andersson, V.B. Golovko, J.F. Alvino, T. Bennett, O. Wrede, S.M. Mejia, H.S. Al Qahtani, R. Adnan, N. Gunby, D.P. Anderson, Phosphine-stabilised Au9 clusters interacting with titania and silica surfaces: The first evidence for the density of states signature of the support-immobilised cluster, J. Chem. Phys. 141 (2014) 014702.

[35] H.S. Al Qahtani, K. Kimoto, T. Bennett, J.F. Alvino, G.G. Andersson, G.F. Metha, V.B. Golovko, T. Sasaki, T. Nakayama, Atomically resolved structure of ligand-protected Au9 clusters on TiO2 nanosheets using aberration-corrected STEM, J. Chem. Phys. 144 (2016) 114703.

[36] Y. Liu, H. Tsunoyama, T. Akita, T. Tsukuda, Preparation of~ 1 nm gold clusters confined within mesoporous silica and microwave-assisted catalytic application for alcohol oxidation, J. Phys. Chem. C 113 (2009) 13457-13461.

[37] W. Zhou, J.M. Thomas, D.S. Shephard, B.F. Johnson, D. Ozkaya, T. Maschmeyer, R.G. Bell, Q. Ge, Ordering of ruthenium cluster carbonyls in mesoporous silica, Science 280 (1998) 705-708.

[38] B. Gates, Supported metal clusters: synthesis, structure, and catalysis, Chem. Rev. 95 (1995) 511-522.

[39] B. Gates, Supported metal cluster catalysts, J. Mol. Catal. A: Chem. 163 (2000) 55-65.

[40] G. Krishnan, N. Eom, R.M. Kirk, V.B. Golovko, G.F. Metha, G.G. Andersson, Investigation of Phosphine Ligand Protected Au13 Clusters on Defect Rich Titania, J. Phys. Chem. C 123 (2019) 6642−6649.

[41] G. Krishnan, H.S. Al Qahtani, J. Li, Y. Yin, N. Eom, V.B. Golovko, G.F. Metha, G.G. Andersson, Investigation of Ligand-Stabilized Gold Clusters on Defect-Rich Titania, J. Phys. Chem. C 121 (2017) 28007-28016.

[42] R. Bennett, C. Pang, N. Perkins, R. Smith, P. Morrall, R. Kvon, M. Bowker, Surface structures in the SMSI state; Pd on (1×2) reconstructed TiO2 (110), J. Phys. Chem. B 106 (2002) 4688-4696.

[43] Q. Fu, T. Wagner, S. Olliges, H.-D. Carstanjen, Metal–oxide interfacial reactions: Encapsulation of Pd on TiO2 (110), J. Phys. Chem. B 109 (2005) 944-951.

[44] A. Berkó, I. Ulrych, K. Prince, Encapsulation of Rh nanoparticles supported on TiO2 (110)-(1×1) surface: XPS and STM studies, J. Phys. Chem. B 102 (1998) 3379-3386.

[45] F.X. Xiao, S.F. Hung, J. Miao, H.Y. Wang, H. Yang, B. Liu, Metal-Cluster-Decorated TiO2 Nanotube Arrays: A Composite Heterostructure toward Versatile Photocatalytic and Photoelectrochemical Applications, Small 11 (2015) 554-567.

[46] I.X. Green, W. Tang, M. Neurock, J.T. Yates, Spectroscopic observation of dual catalytic sites during oxidation of CO on a Au/TiO2 catalyst, Science 333 (2011) 736-739.

[47] A.C. Reber, S.N. Khanna, F.S. Roberts, S.L. Anderson, Effect of O2 and CO Exposure on the Photoelectron Spectroscopy of Size-Selected Pd n Clusters Supported on TiO2 (110), J. Phys. Chem. C 120 (2016) 2126-2138.

[48] H.S. Al Qahtani, G.F. Metha, R.B. Walsh, V.B. Golovko, G.G. Andersson, T. Nakayama, Aggregation behavior of ligand-protected Au9 clusters on sputtered atomic layer deposition TiO2, J. Phys. Chem. C 121 (2017) 10781-10789.

[49] F.S. Roberts, S.L. Anderson, A.C. Reber, S.N. Khanna, Initial and Final State Effects in the Ultraviolet and X-ray Photoelectron Spectroscopy (UPS and XPS) of Size-Selected Pd n Clusters Supported on TiO2 (110), J. Phys. Chem. C 119 (2015) 6033-6046.

[50] J.-Y. Ruzicka, F. Abu Bakar, C. Hoeck, R. Adnan, C. McNicoll, T. Kemmitt, B.C. Cowie, G.F. Metha, G.G. Andersson, V.B. Golovko, Toward Control of Gold Cluster Aggregation on TiO2 via Surface Treatments, J. Phys. Chem. C 119 (2015) 24465-24474.

[51] K. Nakata, S. Sugawara, W. Kurashige, Y. Negishi, M. Nagata, S. Uchida, C. Terashima, T. Kondo, M. Yuasa, A. Fujishima, Cosensitization Properties of Glutathione-Protected Au25 Cluster on Ruthenium Dye-Sensitized TiO2 Photoelectrode, Int. J. Photoenergy 2013 (2013) 456583.

[52] K. Katsiev, G. Harrison, Y. Al-Salik, G. Thornton, H. Idriss, Gold Cluster Coverage Effect on H2 Production over Rutile TiO2 (110), ACS Catal. 9 (2019) 8294-8305.

[53] P. López-Caballero, A.W. Hauser, M.a. Pilar de Lara-Castells, Exploring the Catalytic Properties of Unsupported and TiO2-Supported Cu5 Clusters: CO2 Decomposition to CO and CO2 Photoactivation, J. Phys. Chem. C 123 (2019) 23064-23074.

[54] U. Diebold, The surface science of titanium dioxide, Surf. Sci. Rep. 48 (2003) 53-229.

[55] H. Jensen, A. Soloviev, Z. Li, E.G. Søgaard, XPS and FTIR investigation of the surface properties of different prepared titania nano-powders, Appl. Surf. Sci. 246 (2005) 239-249.

[56] E. Wahlström, N. Lopez, R. Schaub, P. Thostrup, A. Rønnau, C. Africh, E. Lægsgaard, J. Nørskov, F. Besenbacher, Bonding of Gold Nanoclusters to Oxygen Vacancies on Rutile TiO2 (110), Phys. Rev. Lett. 90 (2003) 026101.

[57] I. Hadjoub, T. Touam, A. Chelouche, M. Atoui, J. Solard, M. Chakaroun, A. Fischer, A. Boudrioua, L.-H. Peng, Post-deposition annealing effect on RF-sputtered TiO2 thin-film properties for photonic applications, Appl. Phys. A 122 (2016) 78.

[58] J. Daughtry, A. Alotabi, L. Howard-Fabretto, G.G. Andersson, Composition and Properties of RF-Sputter Deposited Titanium Dioxide Thin Films, Nanoscale Advances 3 (2020) 1077-1086.

[59] A. Haseeb, M. Hasan, H.H. Masjuki, Structural and mechanical properties of nanostructured TiO2 thin films deposited by RF sputtering, Surf. Coat. Technol. 205 (2010) 338-344.

[60] Q. Ye, P. Liu, Z. Tang, L. Zhai, Hydrophilic properties of nano-TiO2 thin films deposited by RF magnetron sputtering, Vacuum 81 (2007) 627-631.

[61] S. Tauster, S. Fung, R.L. Garten, Strong metal-support interactions. Group 8 noble metals supported on titanium dioxide, J. Am. Chem. Soc. 100 (1978) 170-175.

[62] G.L. Haller, D.E. Resasco, Metal–support interaction: Group VIII metals and reducible oxides, Advances in catalysis, Elsevier1989, pp. 173-235.

[63] F. Pesty, H.-P. Steinrück, T.E. Madey, Thermal stability of Pt films on TiO2 (110): evidence for

encapsulation, Surf. Sci. 339 (1995) 83-95.
[64] O. Dulub, W. Hebenstreit, U. Diebold, Imaging cluster surfaces with atomic resolution: the strong metal-support interaction state of Pt supported on TiO 2 (110), Phys. Rev. Lett. 84 (2000) 3646.
[65] R. Bennett, P. Stone, M. Bowker, Pd nanoparticle enhanced re-oxidation of non-stoichiometric TiO2: STM imaging of spillover and a new form of SMSI, Catal. Lett. 59 (1999) 99-105.
[66] Y. Gao, Y. Liang, S. Chambers, Thermal stability and the role of oxygen vacancy defects in strong metal support interaction—Pt on Nb-doped TiO2 (100), Surf. Sci. 365 (1996) 638-648.
[67] H.R. Sadeghi, V.E. Henrich, Electronic interactions in the rhodium/TiO2 system, J. Catal. 109 (1988) 1-11.
[68] H.R. Sadeghi, V.E. Henrich, Rh on TiO2: Model catalyst studies of the strong metal-support interaction, Applications of Surface Science 19 (1984) 330-340.
[69] S. Labich, E. Taglauer, H. Knözinger, Metal–support interactions on rhodium model catalysts, Topics in Catalysis 14 (2000) 153-161.
[70] D. Mullins, K. Zhang, Metal–support interactions between Pt and thin film cerium oxide, Surf. Sci. 513 (2002) 163-173.
[71] Q. Fu, T. Wagner, Metal/oxide interfacial reactions: Oxidation of metals on SrTiO3 (100) and TiO2 (110), J. Phys. Chem. B 109 (2005) 11697-11705.
[72] P.J. Cumpson, Angle-resolved XPS depth-profiling strategies, Appl. Surf. Sci. 144 (1999) 16-20.
[73] C. Wang, G.G. Andersson, Measuring concentration depth profiles at liquid surfaces: Comparing angle resolved X-ray photoelectron spectroscopy and neutral impact collision scattering spectroscopy, Surf. Sci. 605 (2011) 889-897.
[74] L. Óvári, J. Kiss, Growth of Rh nanoclusters on TiO2 (110): XPS and LEIS studies, Appl. Surf. Sci. 252 (2006) 8624-8629.
[75] G. Li, B. Zandkarimi, A.C. Cass, T.J. Gorey, B.J. Allen, A.N. Alexandrova, S.L. Anderson, Sn-modification of Pt7/alumina model catalysts: Suppression of carbon deposition and enhanced thermal stability, J. Chem. Phys. 152 (2020) 024702.
[76] T.J. Gorey, Y. Dai, S.L. Anderson, S. Lee, S. Lee, S. Seifert, R.E. Winans, Selective growth of Al2O3 on size-selected platinum clusters by atomic layer deposition, Surf. Sci. 691 (2020) 121485.
[77] B. Zandkarimi, T.J. Gorey, G. Li, J. Munarriz, S.L. Anderson, A.N. Alexandrova, Alloying with Sn Suppresses Sintering of Size-Selected Sub-Nano Pt Clusters on SiO2 with and without Adsorbates, Chem. Mater. 32 (2020) 8595–8605.
[78] T.J. Gorey, B. Zandkarimi, G. Li, E.T. Baxter, A.N. Alexandrova, S.L. Anderson, Preparation of Size and Composition-Controlled PtnSnx/SiO2 (n= 2, 4, 24) Bimetallic Model Catalysts Using Atomic Layer Deposition, J. Phys. Chem. C 123 (2019) 16194-16209.
[79] E.T. Baxter, M.-A. Ha, A.C. Cass, H. Zhai, A.N. Alexandrova, S.L. Anderson, Diborane Interactions with Pt7/Alumina: Preparation of Size-Controlled Borated Pt Model Catalysts, J. Phys. Chem. C 122 (2018) 1631-1644.
[80] E.T. Baxter, M.-A. Ha, A.C. Cass, A.N. Alexandrova, S.L. Anderson, Ethylene dehydrogenation on Pt4, 7, 8 clusters on Al2O3: Strong cluster size dependence linked to preferred catalyst morphologies, ACS Catal. 7 (2017) 3322-3335.
[81] Y. Dai, T.J. Gorey, S.L. Anderson, S. Lee, S. Lee, S. Seifert, R.E. Winans, Inherent size effects on XANES of nanometer metal clusters: size-selected platinum clusters on silica, J. Phys. Chem. C 121 (2017) 361-374.
[82] F.S. Roberts, M.D. Kane, E.T. Baxter, S.L. Anderson, Oxygen activation and CO oxidation over size-selected Pt n/alumina/Re (0001) model catalysts: correlations with valence electronic structure, physical structure, and binding sites, Phys. Chem. Chem. Phys. 16 (2014) 26443-26457.
[83] M.D. Kane, F.S. Roberts, S.L. Anderson, Mass-selected supported cluster catalysts: Size effects on CO oxidation activity, electronic structure, and thermal stability of Pdn/alumina (n≤ 30) model catalysts, Int. J. Mass Spectrom. Ion Processes 370 (2014) 1-15.
[84] L. Ovári, L. Bugyi, Z. Majzik, A. Berkó, J. Kiss, Surface Structure and Composition of Au−Rh Bimetallic Nanoclusters on TiO2 (110): A LEIS and STM Study, J. Phys. Chem. C 112 (2008) 18011-18016.
[85] C.C. Chusuei, X. Lai, K. Luo, D. Goodman, Modeling heterogeneous catalysts: metal clusters on planar oxide supports, Topics in Catalysis 14 (2000) 71-83.
[86] S.L. Tait, L.T. Ngo, Q. Yu, S.C. Fain Jr, C.T. Campbell, Growth and sintering of Pd clusters on α-Al2O3 (0001), J. Chem. Phys. 122 (2005) 064712.

[87] S. Lee, C. Fan, T.P. Wu, S. Anderson, Agglomeration, sputtering, and carbon monoxide adsorption behavior for Au/Al2O3 prepared by Au-n(+) deposition on Al2O3/NiAl(110), J. Phys. Chem. B 109 (2005) 11340-11347.

[88] J. Kiss, L. Óvári, A. Oszkó, G. Pótári, M. Tóth, K. Baán, A. Erdóhelyi, Structure and reactivity of Au–Rh bimetallic clusters on titanate nanowires, nanotubes and TiO2 (110), Catal. Today 181 (2012) 163-170.

[89] S.A. Tenney, W. He, J.S. Ratliff, D.R. Mullins, D.A. Chen, Characterization of Pt–Au and Ni–Au Clusters on TiO2 (110), Topics in Catalysis 54 (2011) 42-55.

[90] S.A. Tenney, W. He, C.C. Roberts, J.S. Ratliff, S.I. Shah, G.S. Shafai, V. Turkowski, T.S. Rahman, D.A. Chen, CO-induced diffusion of Ni atoms to the surface of Ni–Au clusters on TiO2 (110), J. Phys. Chem. C 115 (2011) 11112-11123.

[91] L. Óvári, A. Berkó, N. Balázs, Z. Majzik, J. Kiss, Formation of Rh−Au Core−Shell Nanoparticles on TiO2 (110) Surface Studied by STM and LEIS, Langmuir 26 (2010) 2167-2175.

[92] Z.-j. Wang, F. Yang, S. Axnanda, C.-j. Liu, D.W. Goodman, Preparation and characterization of Co–Rh bimetallic model catalysts: From thin films to dispersed clusters, Appl. Catal. A 391 (2011) 342-349.

[93] Y. Niu, P. Schlexer, B. Sebok, I. Chorkendorff, G. Pacchioni, R.E. Palmer, Reduced sintering of mass-selected Au clusters on SiO2 by alloying with Ti: an aberration-corrected STEM and computational study, Nanoscale 10 (2018) 2363-2370.

[94] R.P. Galhenage, K. Xie, W. Diao, J.M.M. Tengco, G.S. Seuser, J.R. Monnier, D.A. Chen, Platinum–ruthenium bimetallic clusters on graphite: a comparison of vapor deposition and electroless deposition methods, Phys. Chem. Chem. Phys. 17 (2015) 28354-28363.

[95] H.H. Brongersma, Low-energy ion scattering, Characterization of Materials (2012) 1-23.

[96] H.H. Brongersma, T. Grehl, P.A. van Hal, N.C. Kuijpers, S.G. Mathijssen, E.R. Schofield, R.A. Smith, H.R. ter Veen, High-sensitivity and high-resolution low-energy ion scattering, Vacuum 84 (2010) 1005-1007.

[97] A. Rafati, R. ter Veen, D.G. Castner, Low-energy ion scattering: Determining overlayer thickness for functionalized gold nanoparticles, Surf. Interface Anal. 45 (2013) 1737-1741.

[98] N. Belsey, D. Cant, C. Minelli, J. Araujo, B. Bock, P. Bruener, D. Castner, G. Ceccone, J. Counsell, P. Dietrich, Versailles Project on Advanced Materials and Standards Interlaboratory Study on Measuring the Thickness and Chemistry of Nanoparticle Coatings Using XPS and LEIS, J. Phys. Chem. C 120 (2016) 24070-24079.

[99] V. Jeyalakshmi, R. Mahalakshmy, K. Krishnamurthy, B. Viswanathan, Titania based catalysts for photoreduction of carbon dioxide: Role of modifiers, Indian J. Chem., Sect. A: Inorg., Bio-inorg., Phys., Theor. Anal. Chem. 51A (2012) 1263-1283.

[100] S. Abrahams, J. Bernstein, Rutile: normal probability plot analysis and accurate measurement of crystal structure, J. Chem. Phys. 55 (1971) 3206-3211.

[101] V.N. Popok, I. Barke, E.E.B. Campbell, K.-H. Meiwes-Broer, Cluster–surface interaction: From soft landing to implantation, Surf. Sci. Rep. 66 (2011) 347-377.

[102] J. Castle, A. Salvi, Chemical state information from the near-peak region of the X-ray photoelectron background, J. Electron. Spectrosc. Relat. Phenom. 114 (2001) 1103-1113.

[103] O. Baschenko, A. Nesmeev, The effect of elastic photoelectron scattering on depth-profiling by angular resolved X-ray photoelectron spectroscopy, J. Electron. Spectrosc. Relat. Phenom. 57 (1991) 33-46.

[104] H.H. Brongersma, M. Draxler, M. De Ridder, P. Bauer, Surface composition analysis by low-energy ion scattering, Surf. Sci. Rep. 62 (2007) 63-109.

[105] G. Lu, A. Linsebigler, J.T. Yates Jr, Ti3+ defect sites on TiO2 (110): production and chemical detection of active sites, J. Phys. Chem. 98 (1994) 11733-11738.

[106] W.E. Kaden, W.A. Kunkel, S.L. Anderson, Cluster size effects on sintering, CO adsorption, and implantation in Ir/SiO2, J. Chem. Phys. 131 (2009) 114701.

[107] L.W. Hoffman, G.G. Andersson, A. Sharma, S.R. Clarke, N.H. Voelcker, New insights into the structure of PAMAM dendrimer/gold nanoparticle nanocomposites, Langmuir 27 (2011) 6759-6767.

[108] W.H. Bragg, R. Kleeman, XXXIX. On the α particles of radium, and their loss of range in passing through various atoms and molecules, Lond. Edinb. Dubl. Phil. Mag. 10 (1905) 318-340.

[109] L. Mezey, J. Giber, The surface free energies of solid chemical elements: calculation from internal free enthalpies of atomization, Jpn. J. Appl. Phys. 21 (1982) 1569.

[110] M. Aizawa, S. Lee, S.L. Anderson, Deposition dynamics and chemical properties of size-

selected Ir clusters on TiO2, Surf. Sci. 542 (2003) 253-275.

[111] A. Howard, C. Mitchell, D. Morris, R. Egdell, S. Parker, The surface structure of TiO2 (210) studied by atomically resolved STM and atomistic simulation, Surf. Sci. 448 (2000) 131-141.

[112] S. Tauster, S. Fung, R. Baker, J. Horsley, Strong interactions in supported-metal catalysts, Science 211 (1981) 1121-1125.

[113] S. Bernal, F. Botana, J. Calvino, C. López, J. Pérez-Omil, J. Rodríguez-Izquierdo, High-resolution electron microscopy investigation of metal–support interactions in Rh/TiO 2, J. Chem. Soc., Faraday Trans. 92 (1996) 2799-2809.

[114] S. Bernal, J. Calvino, M. Cauqui, J. Gatica, C.L. Cartes, J.P. Omil, J. Pintado, Some contributions of electron microscopy to the characterisation of the strong metal–support interaction effect, Catal. Today 77 (2003) 385-406.

[115] E. Hebenstreit, W. Hebenstreit, H. Geisler, C. Ventrice Jr, P. Sprunger, U. Diebold, Bulk-defect dependent adsorption on a metal oxide surface: S/TiO2 (110), Surf. Sci. 486 (2001) L467-L474.

[116] T. Komaya, A.T. Bell, Z. Wengsieh, R. Gronsky, F. Engelke, T.S. King, M. Pruski, The influence of metal-support interactions on the accurate determination of Ru dispersion for Ru/TiO2, J. Catal. 149 (1994) 142-148.

[117] T. Sham, T. Ohta, T. Yokoyama, Y. Kitajima, M. Funabashi, N. Kosugi, H. Kuroda, Ru L edge x-ray absorption studies of the electronic structure of Ru3(CO)12 adsorption and the formation of Ru–Cu bimetallics on Cu (111), J. Chem. Phys. 88 (1988) 475-477.

[118] K. Schierbaum, S. Fischer, M. Torquemada, J. De Segovia, E. Roman, J. Martin-Gago, The interaction of Pt with TiO2 (110) surfaces: a comparative XPS, UPS, ISS, and ESD study, Surf. Sci. 345 (1996) 261-273.

[119] M. Della Negra, N.M. Nicolaisen, Z. Li, P.J. Møller, Study of the interactions between the overlayer and the substrate in the early stages of palladium growth on TiO2 (110), Surf. Sci. 540 (2003) 117-128.

[120] H. Feng, J. Lu, P.C. Stair, J.W. Elam, Alumina over-coating on Pd nanoparticle catalysts by atomic layer deposition: enhanced stability and reactivity, Catal. Lett. 141 (2011) 512-517.

[121] W. Kurashige, R. Kumazawa, D. Ishii, R. Hayashi, Y. Niihori, S. Hossain, L.V. Nair, T. Takayama, A. Iwase, S. Yamazoe, T. Tsukuda, A. Kudo, Y. Negishi, Au25-Loaded BaLa4Ti4O15 Water-Splitting Photocatalyst with Enhanced Activity and Durability Produced Using New Chromium Oxide Shell Formation Method, J. Phys. Chem. C 122 (2018) 13669-13681.

[122] S. Vajda, M.J. Pellin, J.P. Greeley, C.L. Marshall, L.A. Curtiss, G.A. Ballentine, J.W. Elam, S. Catillon-Mucherie, P.C. Redfern, F. Mehmood, Subnanometre platinum clusters as highly active and selective catalysts for the oxidative dehydrogenation of propane, Nat. Mater. 8 (2009) 213-216.

[123] Y. Negishi, M. Mizuno, M. Hirayama, M. Omatoi, T. Takayama, A. Iwase, A. Kudo, Enhanced photocatalytic water splitting by BaLa4Ti4O15 loaded with∼ 1 nm gold nanoclusters using glutathione-protected Au25 clusters, Nanoscale 5 (2013) 7188-7192.

[124] T. Yoskamtorn, S. Yamazoe, R. Takahata, J.-i. Nishigaki, A. Thivasasith, J. Limtrakul, T. Tsukuda, Thiolate-mediated selectivity control in aerobic alcohol oxidation by porous carbon-supported Au25 clusters, ACS Catal. 4 (2014) 3696-3700.